PERGAMON

Deep-Sea Research II 48 (2001) 483–499

DEEP-SEA RESEARCH
PART II

www.elsevier.com/locate/dsr2

Evaluating the synopticity of the US GLOBEC Georges Bank broad-scale sampling pattern with observational system simulation experiments☆

D.J. McGillicuddy Jr.[a,*], D.R. Lynch[b], P. Wiebe[c], J. Runge[d], E.G. Durbin[e], W.C. Gentleman[b], C.S. Davis[c]

[a]*Department of Applied Ocean Physics and Engineering, Woods Hole Oceanographic Institution, Woods Hole, MA 02543, USA*
[b]*Dartmouth College, Hanover, NH 03755, USA*
[c]*Biology Department, Woods Hole Oceanographic Institution, Woods Hole, MA 02543, USA*
[d]*Department of Fisheries and Oceans, Maurice-Lamontagne Institute, Division of Ocean Sciences, 850 Route de la Mer, Mont Joli, QC Canada G5H 3Z4*
[e]*Graduate School of Oceanography, University of Rhode Island, Narragansett, RI 02882, USA*

Received 24 November 1998; received in revised form 21 September 1999; accepted 10 December 1999

Abstract

A set of observational system simulation experiments (OSSEs) have been designed to assess quantitatively the synopticity of the broad-scale surveys of Georges Bank carried out as part of the US GLOBEC program. The approach uses model simulations that contain realistic spatial and temporal fluctuations of adult females of the planktonic copepod *Calanus finmarchicus* observed during February and March 1995. Simulations are constructed with two types of assimilation procedures (nudging and the adjoint method), which are used to dynamically interpolate between the two broad-scale surveys taken one month apart. Using these simulations as representations of the real ocean, the model fields are subsampled in space and time along a typical cruise track. These simulated data are then objectively analyzed and the resulting maps compared with "reality" as represented in the original simulation. Results indicate a total error of approximately 50%, which is comprised mostly of simple mapping error (incomplete spatial sampling) and a smaller contribution from space/time smearing. Adjustment of the station positions for displacement by the mean flow reduces the latter error by about half.

☆ Paper published in December 2000.

* Corresponding author. Tel.: 1-508-289-2683; fax: 1-508-457-2194.
E-mail address: dmcgillicuddy@whoi.edu (D.J. Mc Gillicuddy Jr.).

0967-0645/01/$ - see front matter
PII: S0967-0645(00)00126-0

1. Introduction

Biological oceanography is fraught with a particularly difficult sampling problem because there are two distinct sources of space/time fluctuations in organism distributions: heterogeneity in biological processes and stirring by ocean currents. In principle, these two effects would be separable if it were possible to collect a sequence of instantaneous snapshots of both organism abundance and the circulation. Such a situation would lend itself to direct calculation of advective transport, and the biological contribution could be inferred by difference. Of course, practical considerations preclude such an approach; observations are time-consuming and difficult to make at sea, and the speed with which ships can transit between stations is relatively slow. These constraints generally give way to compromise between geographic coverage and resolution in space and time.

The effectiveness of any sampling strategy is ultimately determined by the accuracy with which the observations can be used to reconstruct reality — the state of the natural system being measured. In this context, reality is an elusive metric, for biological distributions in the ocean rarely (if ever) have been oversampled. Given the dearth of opportunity for testing sampling strategies against objective criteria with purely observational means, numerical models offer an attractive framework for investigation of these issues. The approach begins with the construction of a simulation that is characteristic of the natural system. The model run serves as a space/time continuous representation of reality, which is then subsampled in a specified fashion to produce a simulated data set. The simulated data are then fed into an analysis scheme in which they are synthesized into a reconstruction of reality. Direct comparison of the reconstructed field with the "truth" as defined by the original simulation thus provides a quantitative evaluation of that particular sampling strategy. This general procedure, sometimes called observational system simulation experiments (OSSEs), has its origins in dynamic meteorology (e.g. Charney et al., 1969) and is recognized as an important tool for the development of oceanographic sampling systems (Smith, 1993; Robinson et al., 1998).

One aspect of sampling that is particularly amenable to assessment with the OSSE approach is the synopticity of spatial surveys. A set of measurements is synoptic if it is collected in a time interval that is short enough that the underlying distribution does not change appreciably. OSSEs provide a means to quantify the extent to which dynamics in the underlying field can compromise the fidelity of a map generated from data collected over a finite time interval. The procedure consists of the following three steps: (1) subsampling model output along a realistic cruise track over a time interval that reflects the actual time required to occupy those stations at sea, (2) objectively mapping the simulated data, and (3) comparing the analysis with an instantaneous snapshot from the original model calculation. Of course, this estimate of the space/time smearing associated with the sampling strategy is robust only to the extent to which the model simulation used as the basis for the OSSE is representative of the real ocean.

Here we evaluate the synopticity of the US GLOBEC Georges Bank broadscale sampling plan using OSSEs based on data-driven simulations constructed with the Dartmouth finite-element circulation model (Lynch et al., 1996). The approach is to initialize the model with a set of observations and run forward for a period of one month, using a second set of observations as an end point. Two different data assimilation procedures are used to construct these simulations:

nudging and the adjoint method. The forward simulations are then subsampled without error[1] along the broad-scale survey track over the 10-day time period that is required to occupy the sampling grid. The simulated data are then objectively analyzed and compared with truth as defined by an instantaneous snapshot of the model solution at the central time of the survey (day 5.0). The utility of an "advective correction" to the objective analysis reconstruction is investigated by adjusting the locations of the observations from the original stations to their positions at the central time assuming transport by the mean flow.

2. Methods

The US GLOBEC Georges Bank Broadscale Sampling Program was designed to measure seasonal variations in the spatial abundance patterns of the target species (US GLOBEC, 1992; Wiebe et al., 1996a). A typical sampling plan (Fig. 1) consists of approximately 40 stations spread fairly uniformly over the bank. Such a grid takes 10 days to complete. These surveys were occupied monthly from January through June during the years 1995–1999. Station data include CTD profiles of water column properties and abundance estimates for zooplankton and larval fish derived from 1 m^2 and 10 m^2 Multiple Opening and Closing Net and Environmental Sensing Systems (MOCNESS — Wiebe et al., 1985) and Bongo net tows as well as pump profiling for microzooplankton. The OSSEs described herein are based on simulations created using abundance data on adult female *Calanus finmarchicus* derived from MOCNESS tows on two sequential broadscale surveys: R/V *Endeavor* cruises EN261 (10–20 February 1995) and EN263 (13–23 March 1995). Animal concentrations were computed by dividing the vertically integrated abundance estimates by the depth interval that was sampled.

2.1. Objective analysis

Construction of maps suitable for input into models requires an algorithm by which irregularly spaced observations can be interpolated onto an arbitrary grid. Objective analysis is a technique for doing so that minimizes the expected error (in a least squares sense) at each analysis point via a linear combination of the neighboring observations. Each data point is weighted according to its space/time distance from the analysis point and a four-dimensional correlation function derived from the ensemble of prior data. Thus statistical information about the measured field is used to optimize the resulting map. This procedure has been used routinely for nearly three decades in open-ocean applications where the statistics are fairly homogeneous and well-behaved (Bretherton et al., 1976; Freeland and Gould, 1976).

Objective analysis in coastal domains is a much more difficult problem for two reasons. First, the presence of a coastline imposes geometrical constraints that are not easily handled analytically. Second, coastal processes are in general strongly impacted by topography, which results in highly non-uniform statistics. For example, Petrie and Dean-Moore (1996) demonstrated that correlation

[1] Incorporation of measurement error would enhance the realism of this exercise; we have chosen not to do so in order to focus attention on the space/time smearing issue.

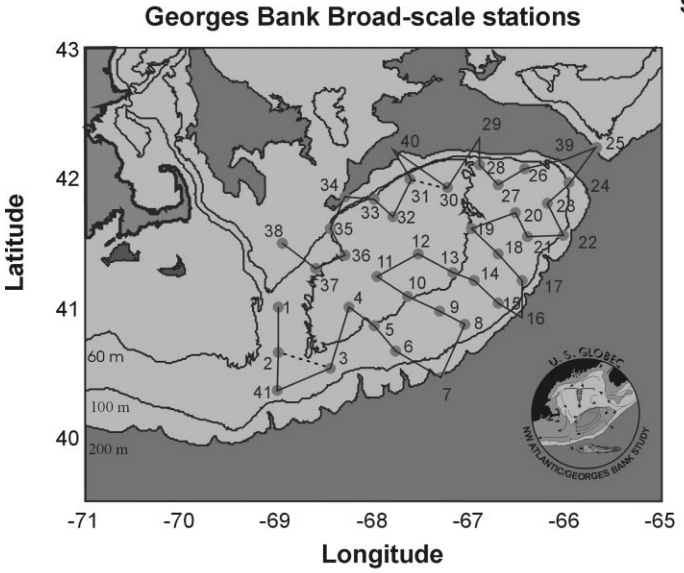

Georges Bank Broad-scale Sampling Scheme	Consecutive Station Numbers for 1996
1-25	1-25
39	26
26	27
27	28
28	29
29	30
30	31
31	32
32	33
33	34
34	35
35	36
36	37
37	38
38	39

40 not occupied in 1996
41 not occupied in 1996

Fig. 1. The US GLOBEC Georges Bank Program broad-scale sampling station plan for 1998. The first broad-scale sampling was conducted in June 1994 with a sampling design (with 48 stations) that was subsequently modified into a pattern that was used in 1995 and had 38 stations. Station 39 was added during the 1996 field season, Station 40 was added in 1997, and Station 41 was added in 1998. Dashed lines indicate where cruise tracks prior to 1998 differ due to these changes in the station plan. The accompanying table provides a conversion between GLOBEC station identifiers and the sequential numbering scheme used in the text and Figs. 3, 4 and 6.

scales of physical properties on the Scotian shelf were generally larger in the along-isobath direction than across isobaths. He et al. (1997) have implemented these aspects into an objective analysis procedure based on the original algorithm developed by Bretherton et al. (1976). The basic idea is that a set of domain-wide correlation scales are modulated by the local bathymetric gradients, such that the anisotropy with respect to along versus across isobath correlations is explicit. The domain-wide covariance model used here is of the form

$$\mathrm{Cov}(C_i, C_j) = \sigma^2 \mathrm{e}^{-r}\left(1 + r + \frac{r^2}{3}\right),$$

where σ^2 is the variance estimated from the data and r is the pseudo-distance between points i and j defined as

$$r = \sqrt{\left(\frac{\Delta x'}{S_{x'}}\right)^2 + \left(\frac{\Delta y'}{S_{y'}}\right)^2 + \left(\frac{\Delta t}{S_t}\right)^2}$$

in which the coordinates x' and y' refer to the local cross-isobath and along-isobath directions, respectively. The scale factors are oriented with respect to the local topography in the following

manner,

$$S_{x'} = S_0(1 - C_x\sqrt{s}), \quad S_{y'} = S_0(1 + C_y\sqrt{s}),$$

where s is the magnitude of the bathymetric gradient. For the purposes of this study, the same correlation scales were used to map zooplankton distributions as were used in the objective analysis of hydrographic measurements used to drive the circulation model (see below): $S_0 = 30$ km, $C_x = 3$, $C_y = 10$ and a temporal scale $S_t = 30$ days. Sensitivity analysis showed that the resulting maps of zooplankton distributions on Georges Bank were generally robust over a range of choices for the global correlation scales. However, rigorous assessment of the spatial and temporal covariance statistics of the target species is clearly needed in future research.

2.2. Simulation model

The circulation in this region has been the subject of intense modeling activity by the Dartmouth Numerical Methods Laboratory (Lynch et al., 1996). A finite element approach has been utilized that facilitates realistic representation of the complex geometry in this area. Horizontal grid spacing in regions of steep topography is as fine as 500 m, and considerably coarser where such high resolution is not required. Perhaps the most relevant circulation element in the present problem is the clockwise flow around Georges Bank, caused by both tidal rectification and baroclinic effects. This aspect of the physical solutions has a scale of the same order as the biological sampling. Thus, the physical and biological scales resolved in this coupled problem are reasonably well matched.

This three-dimensional model is hydrostatic, non-linear, and incorporates advanced turbulence closure. Published solutions for the climatological mean circulation, broken down into six bi-monthly periods, are demonstrably consistent with available observations (Naimie, 1996; Naimie et al., 2001). Archived solutions are stored in a form that is available for use in an off-line transport code "Acadia", which solves a depth-integrated form of the advection–diffusion-reaction equation on the same grid using the archived hydrodynamic information as input.

Within this framework, the coupled physical–biological model for vertically averaged zooplankton concentration C is written

$$\frac{\partial C}{\partial t} + \mathbf{v}\cdot\nabla C - \frac{1}{H}\nabla\cdot(HK\nabla C) = R, \tag{1}$$

where $\mathbf{v}$ is the velocity, K the diffusivity, H the bottom depth, and R the biological "reaction" term. Positive R implies net growth of the population, while negative R implies net mortality. Climatological mean velocity and diffusivity fields are specified from the bi-monthly archive described above. Boundary conditions consist of (1) no flux through solid boundaries, (2) specification of concentration at inflow, and (3) computation of concentration at outflow assuming no diffusive flux.

2.3. Construction of realistic simulations

The OSSEs described herein are based on simulations that match observed *Calanus finmarchicus* concentrations at two points in time. Distribution maps at the two time points are derived from

objectively analyzed broadscale surveys. The matching is achieved by adjustment of the biological reaction term R in Eq. (1). Two different approaches are used: nudging and the adjoint method. These two assimilation procedures are discussed in turn below.

Nudging is a technique of data assimilation in which a model state variable is relaxed to a particular value via a first-order process. For the present purposes, the simulation is initialized with the concentration field derived from an objective analysis of the first survey (EN261), and then nudged toward an objective analysis of the subsequent observations (EN263). In Eq. (1) above, this amounts to $R = -\alpha(C - C_{\mathrm{obs}})$, where α is the nudging parameter and C_{obs} is the concentration observed in the second survey. The rate constant of the relaxation thus specifies the e-folding time scale at which the model solution converges. At steady state, the nudging term balances the model's local tendency to drift away from the observed value. Thus the stiffness of the nudging controls not only the time scale for convergence, but also the magnitude of the steady-state difference between the numerical solution and the observations.

A series of experiments were conducted in order to determine an appropriate value for the nudging parameter. Our aim is to simulate a 10-day period (the time it takes to complete a survey) in which the temporal changes are realistic. Fig. 2 shows time series of the differences between model solutions and the data toward which they being nudged for three different values of the nudging parameter. The solid line indicates the "ideal" solution for these purposes, which is a monotonic trajectory between the two observational periods. Clearly the nudging simulations produce exponential rather than monotonic adjustment from the initial conditions.[2] However, the relatively linear change in the first 10 days of simulation (c) are actually quite close to "ideal", as this term has been defined here. A value of $\alpha = 40\ \mathrm{days}^{-1}$ is therefore used in the nudging experiments described below.

Adjoint data assimilation provides a more sophisticated (and arguably more realistic) approach to creating a simulation of the type needed here. This technique facilitates inversion for the population dynamics implied by the changes in abundance between the two surveys and the circulation during the intervening period. The method begins with the definition of a cost function, which is a measure of the misfit between predicted and observed concentrations. The goal of the procedure is to minimize the cost function subject to the constraints that the forward model equations are obeyed. Formulation of a Lagrange function, which is the sum of the cost function and the product of a set of Lagrange multipliers with the model equations, facilitates derivation of the adjoint model. For the case in which the biological reaction term is a spatially varying constant $R = R(x, y)$, the adjoint of Eq. (1) is

$$-\frac{\partial \lambda}{\partial t} - \nabla\cdot(\lambda \mathbf{v}) - \frac{1}{H}\nabla\cdot(HK\nabla\lambda) = -2\delta_{\mathrm{M}}(C - C_{\mathrm{obs}}), \tag{2}$$

where λ are the Lagrange multipliers and δ_{M} is a measurement functional that is equal to one where observations exist in space–time and zero elsewhere. Dynamically analogous to the forward model, the adjoint model is an advection–diffusion-reaction equation that describes the propagation of information about model-data misfits. It can be shown that integration of the adjoint equation provides a method of computing the gradient of the cost function with respect to the unknown

[2] Note that non-zero asymptotes in this family of curves demonstrate the strong role of advection in these solutions.

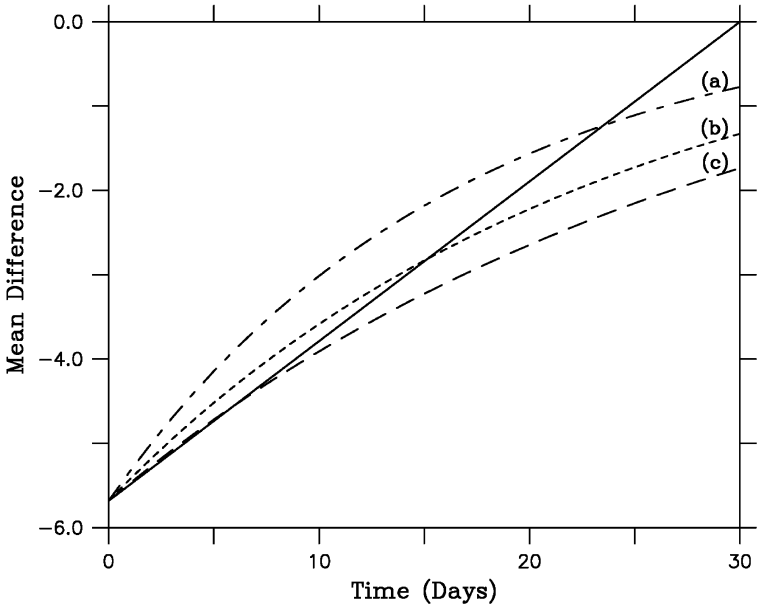

Fig. 2. Time series of the differences between model solutions and the data toward which they being nudged for three different experiments in which the relaxation time scales are (a) 20, (b) 30 and (c) 40 days. The trajectory of monotonic convergence to the second set of observations is indicated by the solid line.

variable $R(x, y)$.[3] This provides the basis for a iterative solution to the variational problem which consists of the following steps: (1) starting with some initial guess of the unknown variable (e.g., $R = 0$), initialize with data from the first survey and run forward in time to evaluate the cost function; (2) integrate the adjoint model, forced by the misfit between observed and predicted values to evaluate the gradient of the cost function with respect to the unknown variable; (3) feed the cost function and its gradient into a descent algorithm to produce an updated estimate of $R(x, y)$; and (4) repeat as necessary until convergence is attained. In practice, the assimilation procedure produces solutions that are nearly identical to the observations. See McGillicuddy et al. (1998) for more details on the method and its application to *Pseudocalanus* spp. populations in the Georges Bank — Gulf of Maine region.

For the present purposes, either of these simulations — nudging or adjoint — are taken as reasonable surrogates for the natural system. This is demonstrated below. The two simulations represent two equally plausible population dynamics scenarios, in which the animal distribution changes in a manner that the broad-scale survey is intended to resolve. An effective sampling plan at least should be successful with these two versions of reality.

[3] In this particular application, all of the model-data misfits are attributed to biological processes. Thus, the assimilation procedure will amalgamate any errors in the prescribed circulation into the inversion for $R(x, y)$. The implicit assumption here is that errors in the physics are small relative to biological sources and sinks.

2.4. Experimental design

The OSSEs described below consist of three separate experiments that are performed on each case. First, the model simulation is sampled on the central date (day 5.0) as if the ship were able to occupy all 39 stations instantaneously. This serves as the control in which the simulated observations are perfectly synoptic. Differences between an objective analysis of the simulated observations and the "true" field (day 5.0 of the model simulation) are thus a result of mapping error only. Second, the model simulation is sampled in space and time during days 1–10 along the prescribed broadscale sampling pattern (see Table 1 for sampling schedule). In this case, differences between the objective analysis of the simulated observations and day 5.0 of the original simulation are a combination of mapping error and the spatial/temporal smearing inherent in the sampling plan. The magnitude of the difference between this and the control experiment is thus a measure of the error associated with the lack of synopticity. Finally, the space/time experiment is repeated with the station positions adjusted (relative to the central time) for the fluid displacement by the mean current. That is, the locations of stations occupied prior to day 5 are advected forward, those on day 5 are unaffected, and those after day 5 are advected backward. Comparison of the objective analysis using the adjusted data with the prior experiment thus facilitates evaluation of an advective correction aimed at reducing spatial/temporal smearing.

Each of the three experiments is performed on several simulations based on the EN261/EN263 MOCNESS data. Sensitivity experiments are performed with respect to the flow field and the representation of population dynamics used in the simulations. Ascertaining the sensitivity of the results to the flow field is of particular interest because the timing of the observations is such that they straddle the boundary between periods for which the climatological flow is archived (January–February and March–April). Sensitivity to the method of biological data assimilation is

Table 1
Sampling schedule for the 1995 US GLOBEC Georges Bank broad-scale surveys[a].

Sampling day	Stations occupied
0	1
1	2–5
2	6–9
3	10–13
4	14–17
5	18–21
6	22–25
7	26–29
8	30–33
9	34–37
10	38–39

[a]Note that the station numbering here (and in Figs. 3, 4 and 6) is sequential; see Fig. 1 for a conversion to GLOBEC station identifiers.

Table 2
Run table and error summary for the observational system simulation experiments[a].

Base simulation			OSSE experiments		
No.	Method	Flow	Control	Space/time	Adv. corr.
1	Nudging	JF	0.212	0.296	0.241
2	Nudging	MA	0.222	0.295	0.209
3	Adjoint	JF	0.508	0.561	0.553
4	Adjoint	MA	0.554	0.596	0.570
Mean: exps. 1–4			0.374	0.437	0.393

[a]Results are presented in terms of the normalized root mean square difference between objective analyses of simulated data and "truth" defined as day 5.0 of the model simulation on which each set of experiments are based. The values shown here represent an areal average of the gridded fields on Georges Bank, for the waters inside the 100 m isobath and east of the 69 W meridian which cuts through the Great South Channel. JF refers to January–February, and MA to March–April.

relevant in that the results of neither technique have been verified with biological measurements of associated source/sink terms; in the absence of such information it is not possible to determine which technique is more appropriate. In all, four sets of the three experiments each were performed (Table 2).

3. Results and discussion

Objective analysis of the EN261 and EN263 data reveals a great deal of structure in the distribution of adult female *C. finmarchicus* (Fig. 3a and b). In the February survey, four distinct maxima in abundance are present: on the northeast peak, the northeast portion of the crest just inside the 60 m isobath, the center of the crest, and just north of the Great South Channel. In addition, there is a broad region of low concentration south of the crest. The March survey is characterized by a north–south band of very high abundance that cuts across the center of the bank; although it is quite coherent, local maxima are clearly evident within the band. It is flanked by large areas of relatively low concentration to the east and west. The peak in abundance present just to the north of the Great South Channel in February appears to have intensified.

Two different data assimilation techniques were used to create simulations of the time period in between the two surveys. Nudging is an inherently local process, so the structure of the forcing term arising from this procedure reflects the Eulerian difference between the evolving concentration field and the terminal condition toward which the solution is being nudged. Strong sources to the north and south of the peak at station 31[4] build up the meridional band of high concentration (Fig. 3c).

[4] Note that in this discussion we use a chronological numbering scheme which reflects the order in which the stations are occupied at sea. See Fig. 1 for a conversion to Globec station identifiers.

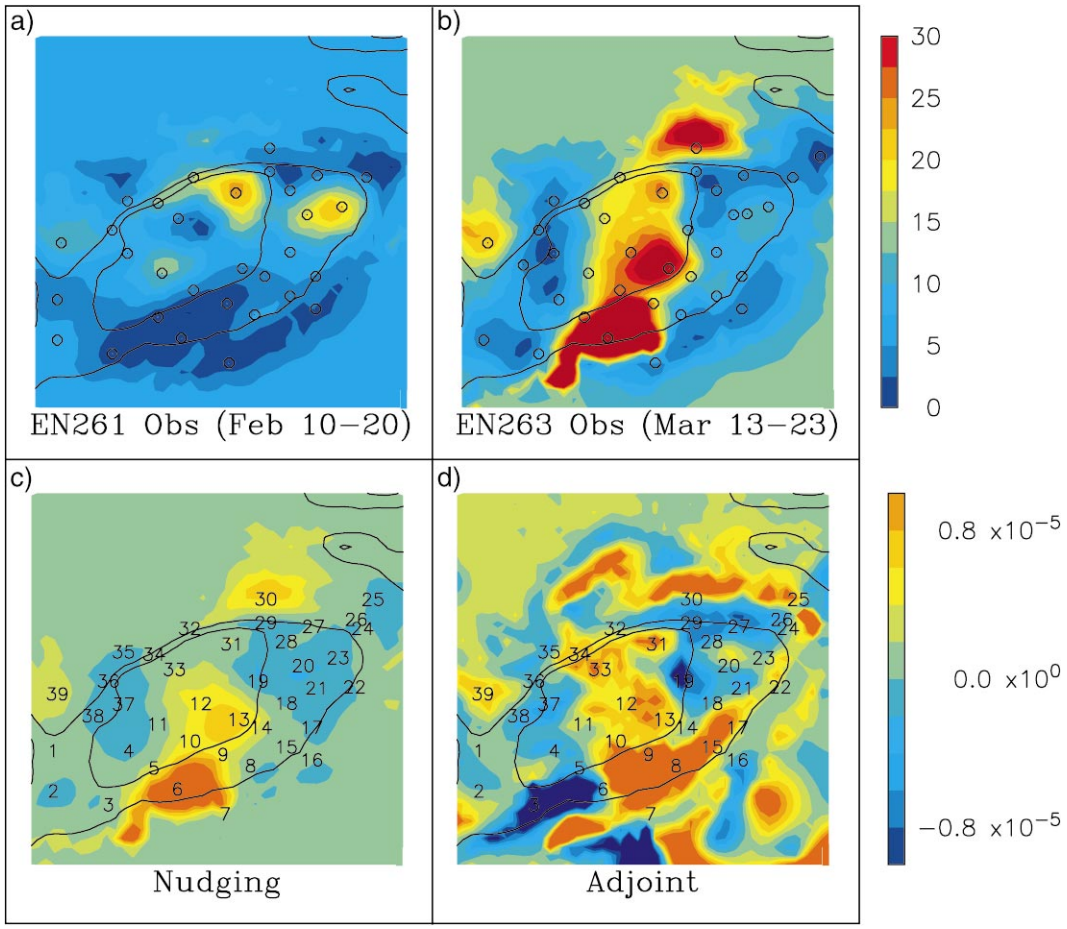

Fig. 3. Objective analyses of adult female *C. finmarchicus* abundance (number of animals m^{-3}) observed during cruises (a) EN261, and (b) EN263. Shown below are the source terms (number of animals m^{-3} s^{-1}) used to create a simulation of the time period between the two cruises using nudging (c) and the adjoint method (d). The nudging term in panel (c) is averaged over the time period of the simulation. These two fields correspond to the flow field for January–February; results using the March–April flow are quite similar and therefore not shown here. Note that the locations of the observations in the top two maps (indicated by circles) do not exactly match each other or the station positions called for in the broad-scale sampling plan (depicted by numerals in the lower two panels; see also Fig. 1); such discrepancies are unavoidable during normal seagoing operations. The 60 and 100 m isobaths are overlayed on all panels. Note that the station numbering is sequential; see Fig. 1 for a conversion to GLOBEC station identifiers.

Sinks to the east and west maintain low concentrations in those regions, while a weak source north of the Great South Channel is responsible for amplification of the peak in that area. In contrast, the adjoint method explicitly represents the effects of the fluid transport in the construction of the biological reaction term (Fig. 3d). Net sources occur upstream of areas in which abundance increases, whereas net sinks are required where high concentrations are advected into regions where the animals are not observed. A prime example of this occurs along the southern flank of the

bank, where strong southwestward flow is present. Buildup of the peak in the vicinity of station 6 is brought about by net growth upstream (to the northeast), and net mortality downstream (to the southwest). In other areas where the mean current is weak, changes in abundance are largely controlled by local balances. In such circumstances, the source term computed with the adjoint method resembles the nudging solution. Examples include the net growth present near stations 11–12 and 39, and the net mortality which straddles the 60 m isobath northeast of the Great South Channel.

Biological rates implied by the distribution of sources and sinks created by the two assimilation procedures are not unrealistic. The magnitude of the reaction term varies from about -1 to $+1$ individual m^{-3} day^{-1}. Note that this is an absolute rate of population change, not a specific rate. Interpreting positive R (a source) as molting of C5 copepodites to adults, the rate of 1 individual m^{-3} day^{-1} is plausible based on the abundance of C5s on Georges Bank at this time (data not shown; see the US GLOBEC Georges Bank Zooplankton Home Page at http://globec.gso.uri.edu/) and temperature-dependent development (Belehradek, 1935; see also Lynch et al., 1998). Negative R implies net mortality in the adult population; consumption of 1 individual m^{-3} day^{-1} is easily justifiable in terms of the abundance of predators and rates of ingestion measured on Georges Bank (Davis, 1984; Sullivan and Meise, 1996; Madin et al., 1996). Thus, from the point of view of biological rates, both the nudging and adjoint solutions are reasonable candidates for realistic simulations.

Results of the first set of experiments (Table 2) are presented in Fig. 4. Animations of the simulated space/time sampling are available on the accompanying CD-ROM and also at http://science.whoi.edu/users/mcgillic/globec/OSSE_paper/animations/. The base simulation was created with nudging using the January/February flow field. The top row of panels shows three instantaneous snapshots of simulated abundance during the first 10 days of integration. Note that the first panel (Sim Day 0) is identical to the objective analysis of the EN261 survey (Fig. 3a), as it was used for the initial condition. In the control experiment, simulated measurements are collected from an instantaneous occupation of stations 1–39 on day 5. The resulting objective analysis and its difference field with the "reality" as defined by the simulation on day 5 reveal that the general features of the distribution have been captured. The most significant discrepancies are associated with (1) smoothing of the peaks near stations 11, 21 and 39; and (2) fine scale structure in the "true" field that is not resolved by the sampling. The most obvious example of the latter occurs at the western end of the southern flank, where a local minimum develops in the simulation in between stations 2 and 3.

Comparison with the experiment in which the model is sampled during days 0–10 along the cruise track reveals the additional error that arises from spatial and temporal smearing associated with the lack of synopticity. The most prominent example occurs in the vicinity of stations 3, 5 and 6, where a local minimum present in the initial condition turns into a local maximum by day 10. Because this area is sampled early in the survey (days 1–2), the resulting objective analysis depicts a local minimum there. The difference field in the region thus reflects an underestimate of the "truth" in model day 5, which is characterized by intermediate concentrations in that area. Another notable example of smearing is evident in the further reduction of the peak concentration around station 31. During the simulation, the peak is advected southward and decreases in magnitude. Because those stations are occupied late in the survey (day 8), the simulated measurements (and therefore the resulting objective analysis) reflect the degraded peak.

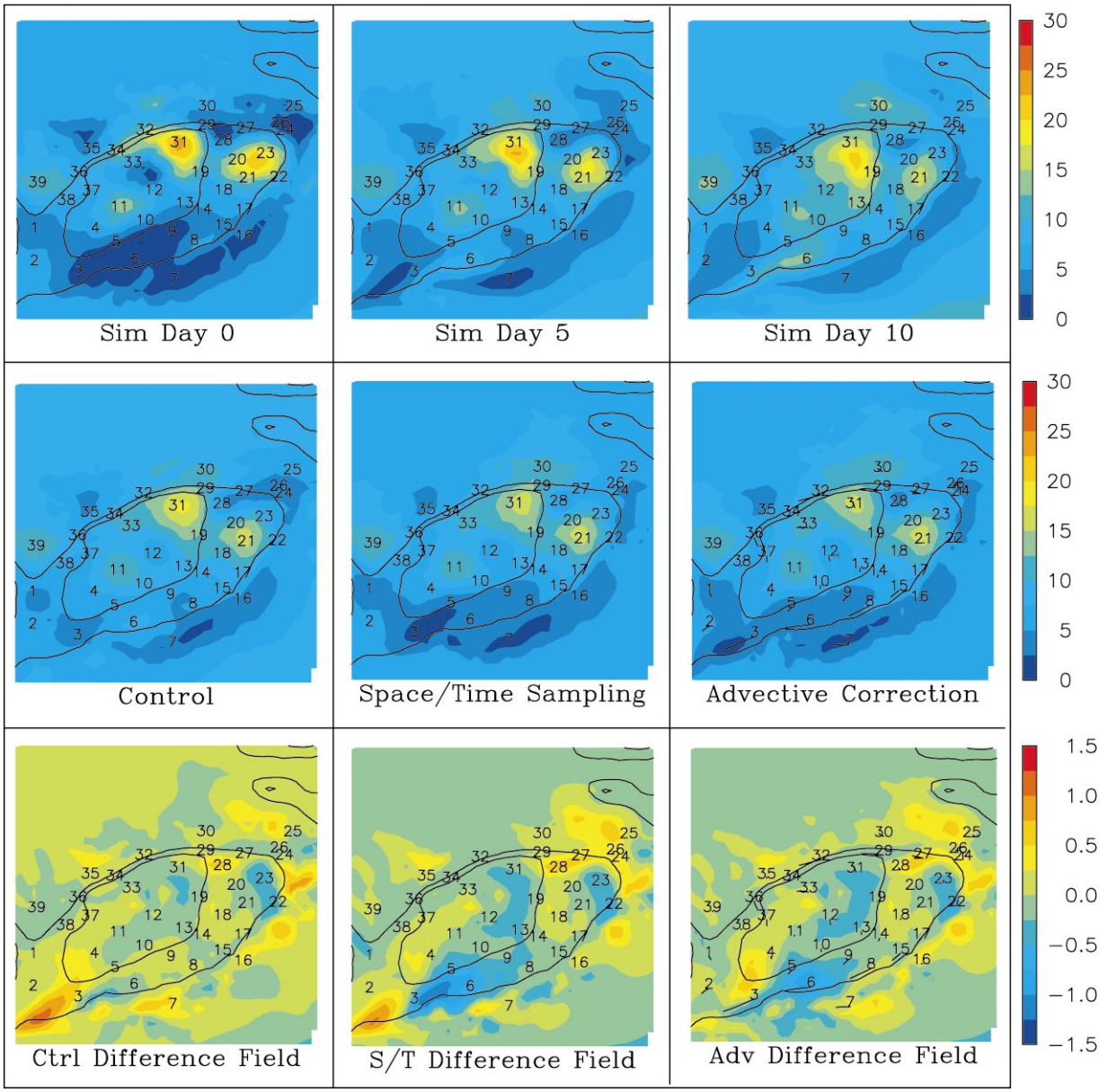

Fig. 4. Observational system simulation experiments using the EN261/EN263 data and the nudging technique with the January/February flow field. The top row shows three snapshots of the simulation representing "truth". These maps are a subregion of a much larger model domain extending from the New England Shelf up through the Gulf of Maine to Nova Scotia (for more information see Lynch et al. (1998)). The middle row shows objective analyses of simulated data from each of the three experiments described in the text. Difference fields with "truth" (defined as day 5 of the model simulation) for each experiment are displayed in the bottom row. Station locations are indicated by numerals; the displacement of the observations associated with the advective corrections are shown in the lower two panels of the right hand column. Units for all panels are number of animals m^{-3}. Note that the station numbering is sequential; see Fig. 1 for a conversion to GLOBEC station identifiers.

Correcting the station positions for advection by the mean flow helps reduce the impact of space/time smearing. In particular, southwestward advection of stations 3 and 6 noticeably improves the objective analysis along the western portion of the southern flank. In the first few days of the simulation (during which this region is sampled), the broad area of low concentration around stations 3, 5, 6 and 9 is neutralized by the nudging term seeking to create the maximum that accumulates there one month later. The advective correction improves the analysis here in two ways. First, the local minimum in between stations 2 and 3 on day five of the simulation is recreated almost perfectly by the advective correction: because station 3 does not lie within the region of positive nudging, the westernmost portion of the low-concentration water breaks off and is swept to the southwest. Accordingly, repositioning the simulated observation at station 3 places the subgridscale local minimum right where it should be. The second improvement relates to the southwestward displacement of the simulated observation at station 6, where the maximum in positive nudging is located. Advection of the increased concentration toward station 3 helps flatten out the minimum there, resulting in improvement of the difference field in a strip-oriented northeast–southwest in between stations 3 and 5.

In an attempt to assess the sensitivity of these results to the specified circulation, the experiments were repeated using the climatological flow from the March/April period. The resulting maps were qualitatively similar to Fig. 4 and therefore are not shown here. Only minor differences are evident between the January/February and March/April experiments in terms of their root mean square differences with "truth" integrated over the bank (Fig. 5a).

Simulations based on the adjoint method show more dramatic evolution in the first 10 days than the nudging runs. The case using the January/February flow field (Fig. 6) reveals a higher dynamic range in concentration values over the same time period, as well as more fine structure. In terms of the bank-wide structure, the biggest differences with the nudging case occur along the southern flank. The strip of net growth from just east of station 6 all the way to station 17 (Fig. 3d) causes

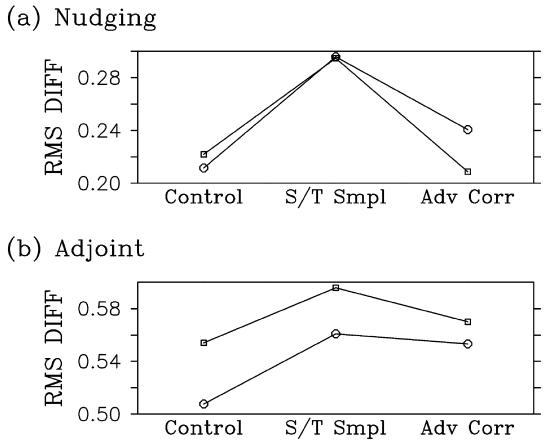

Fig. 5. Normalized root mean square difference between objective analyses of simulated data and "truth" averaged over Georges Bank (see Table 2 caption for definitions). Panels (a) and (b) pertain to the experiments based on EN261/EN263 data using nudging and the adjoint method, respectively. Circles represent results using the January/February flow field, and squares March/April.

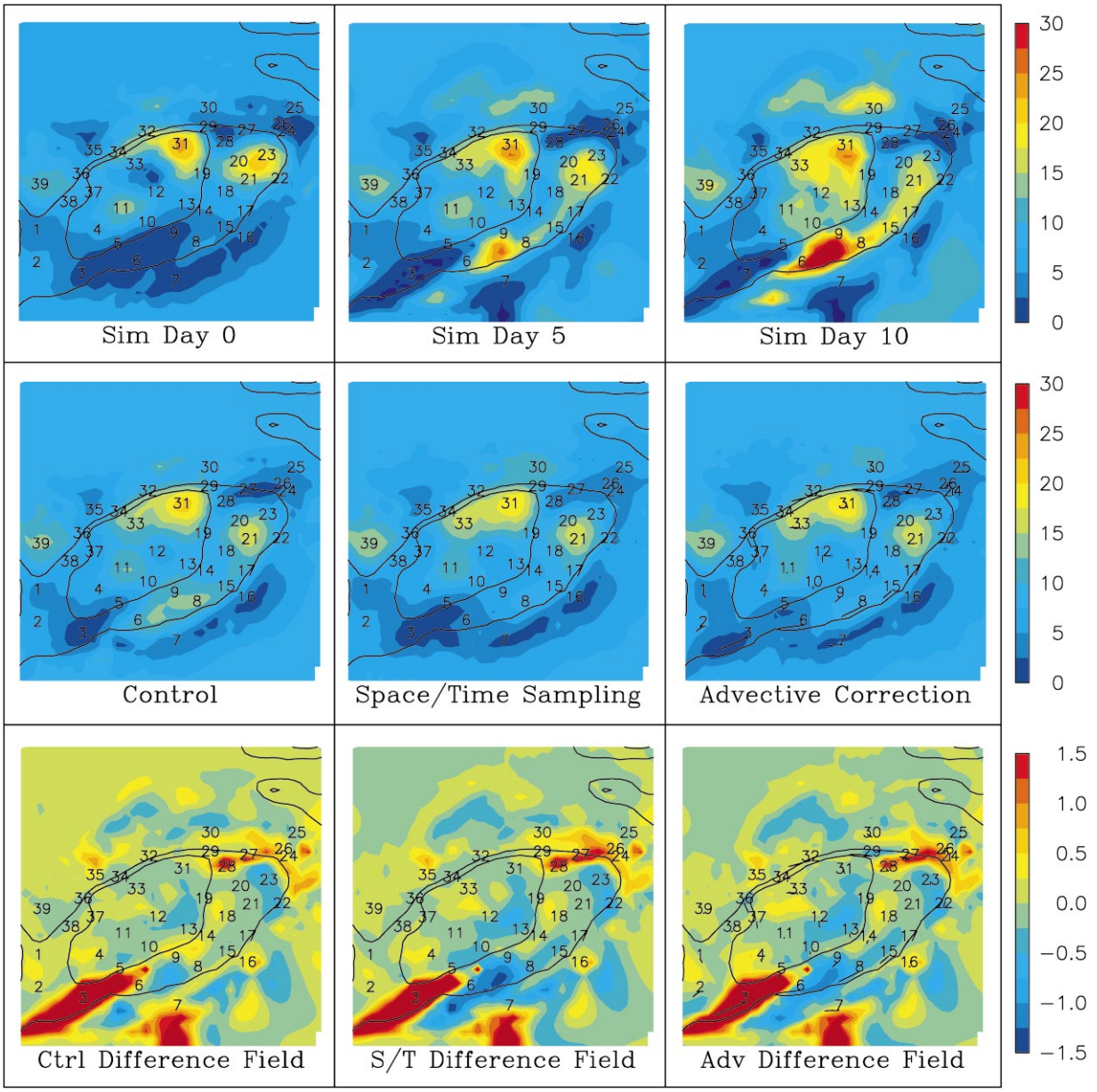

Fig. 6. Same as Fig. 4, but the simulation on which the experiments are conducted is based on the adjoint method.

strong accumulation there, which is most intense furthest downstream. As it turns out, the local maximum in that region is located in between stations 6, 7, 8, and 9 on day 5 (model "truth"). Because only the periphery of the peak is sampled, the concentration in that area is underestimated even in the perfectly synoptic control experiment. That issue aside, the general features of the bank-wide distribution are represented, including the peaks in the vicinities of stations 11, 21, 31

and 39. However, there is in general more fine structure in between stations than in the nudging cases, thereby increasing the overall magnitude of the mapping error quantified by the control experiment (Fig. 5b).

Spatial and temporal smearing associated with occupation of the ship track further degrades the fidelity of the objective analysis. Sampling of stations 6–9 early in the survey (day 2) causes the concentration to be underestimated there. Another noticeable difference with the control experiment occurs on the eastern side of the north flank, where a small patch of low-concentration water originating between stations 27, 28 and 29 is transported to the very edge of the northeast peak during the 10 days of simulation. On day 5, the patch is centered on station 27. However, station 27 is not occupied until day 7, just after the low has passed; this results in an overestimate of the concentration there.

Correcting the station positions for the mean flow causes little change in this case. Some areas are improved slightly. For example, southwestward displacement of the simulated observation at station 3 helps partially compensate for the unresolved minimum in between there and station 2. However, averaged over the bank the improvement is very minor (Fig. 5b).

As in the nudging cases, basing the experiments on the March/April flow field causes little change in the qualitative behavior, and so the detailed maps are not presented here. But, there is a significant increase in the magnitude of the mapping error (Fig. 5b), owing to the creation of more fine-scale structure in the March/April case. The increased mapping error is carried over into the space/time sampling and advective correction experiments, but again the qualitative sense of the results is the same.

4. Conclusions

The Observational System Simulation Experiments described herein present a framework in which some of the error characteristics of the US GLOBEC Georges Bank broadscale sampling plan can be investigated. The results indicate that the largest source of error is associated with the mapping procedure itself: perfectly synoptic surveys of instantaneous model-generated fields result in normalized root mean square errors that range between 22% (for the nudging cases) and 53% (for the adjoint cases). In essence, the mapping error is a measure of the degree to which the sampling grid resolves the "true" variability. In these experiments, the adjoint data assimilation procedure creates more subgridscale structure in the model simulations used to represent reality, and the mapping error is commensurately higher. Space/time smearing associated with the lack of synopticity increases the overall error to 30% (nudging) and 58% (adjoint). As a percentage of the mapping error, this amounts to 36 and 9% for the nudging and adjoint cases, respectively. Thus the relative error caused by space/time smearing is more pronounced in the case where the "biological" forcing used to create the simulation is inherently local (nudging). In that instance, correcting the station positions for advection by the mean flow is particularly effective, reducing the additional space/time smearing error by approximately 80%. The advective correction is less powerful (35% reduction) when the dynamics underlying the production of variability are not local, as in the adjoint method. Averaging all the cases together, there is a mapping error of approximately 40% in perfectly synoptic sampling; space/time smearing contributes an additional 20% (as a percentage of the mapping error), of which about half can be recovered through advective corrections.

There are several important caveats that must be considered in interpreting these results. First, the OSSEs are based on simulations constructed from data that were collected using the same sampling pattern being tested for robustness. Thus the "true" fields contain features that may have been smeared by the exact same sampling problems addressed here. Furthermore, they may not adequately represent variations that are not resolved by the grid. Skewness in the statistics of patchiness structure and its scale dependence has significant implications with respect to resolving larger-scale population distributions (Pinel-Alloul and Pont, 1991; Cyr et al., 1992). We plan to investigate the issues of sampling error and subgridscale patchiness in future work, using high-resolution data based on acoustical techniques (Wiebe et al., 1996b) and the Video Plankton Recorder (e.g., Davis et al., 1996). Suffice it to say that the present OSSEs are biased in favor of the sampling scheme, having already favorably filtered the observational basis of the simulated "truth". Therefore, these experiments are more a test of the internal consistency of the sampling scheme than an absolute assessment of its accuracy.

Of course, these checks for internal consistency are based on representations of reality that may have their own intrinsic physical and biological shortcomings. Although the sensitivity of the results to some aspects have been assessed (i.e. choice of bimonthly flow field and data assimilation method), the possibility of systematic deficiencies in the simulations cannot be discounted. Examples include storm-driven washout events in which departures from the climatological flow can be quite large, and the role of vertical shear and biological behavior in controlling organism distributions. Perhaps of even more concern is the prospect that even subtle errors in the circulation could give rise to unrealistic behavior of the coupled system. It is important to remember that the OSSEs described herein are applicable only to the extent to which the baseline simulations represent reality.

Finally, these results are based on one particular stage of one species during one time period. While the basic aspects of the space/time mapping problem may be somewhat general, their manifestation in other circumstances could be quite different. However, subject to the caveats discussed above, this study suggests that the error contribution from the lack of synopticity in the broad-scale surveys is smaller than the simple mapping error associated with under-resolution of spatial patterns. Taken together, these two sources result in an average error of approximately 50% in abundance maps. This estimate represents a lower bound in that there are additional sources of error which were not included in this analysis.

Acknowledgements

Support of this work by the National Science Foundation is greatly appreciated. This is WHOI contribution 10018 and US GLOBEC contribution 124.

References

Belehradek, J., 1935. Temperature and living matter. Protoplasma Monographs 8, 1–277.

Bretherton, F., Davis, R., Fandry, C., 1976. A technique for objective analysis and design of oceanographic experiments applied to Mode-73. Deep-Sea Research 23, 559–582.

Charney, J., Halem, M., Jastrow, R., 1969. Use of incomplete historical data to infer the present state of the atmosphere. Journal of Atmospheric Science 26, 1160–1163.

Cyr, H., Downing, J., Lalonde, S., Baines, S., Pace, M., 1992. Sampling larval fish populations: choice of sample number and size. Transactions of the American Fisheries Society 121, 356–368.

Davis, C., 1984. Predatory control of copepod seasonal cycles on Georges Bank. Marine Biology 82, 31–40.

Davis, C., Gallager, S., Marra, M., Stewart, W., 1996. Rapid visualization of plankton abundance and taxonomic composition using the video plankton recorder. Deep-Sea Research II 43, 1946–1970.

Freeland, H., Gould, W., 1976. Objective analysis of meso-scale ocean circulation features. Deep-Sea Research 23, 915–923.

He, I., Hendry, R., Boudreau, G., 1997. OAX demonstration and test case. http://www.tuns.ca/ ~ hey/ocean/oview.html.

Lynch, D., Gentleman, W., McGillicuddy, D., Davis, C., 1998. Biological/physical simulations of *Calanus finmarchicus* in the Gulf of Maine. Marine Ecology — Progress Series 169, 189–210.

Lynch, D., Ip, J., Naimie, C., Werner, F., 1996. Comprehensive coastal circulation model with application to the Gulf of Maine. Continental Shelf Research 16, 875–906.

Madin, L., Bollens, S., Horgan, E., Butler, M., Runge, J., Sullivan, B., MacPhee, G., Durbin, E., Durbin, A., Van Kueren, D., Plourde, S., Bucklin, A., Clarke, M., 1996. Voratious planktonic hydroids: unexpected predatory impact on a coastal marine ecosystem. Deep-Sea Research II 43, 1823–1829.

McGillicuddy, D., Lynch, D., Moore, A., Gentleman, W., Davis, C., Meise, C., 1998. An adjoint data assimilation approach to diagnosis of physical and biological controls on *Pseudocalanus* spp. in the Gulf of Maine — Georges Bank region. Fisheries Oceanography 7, 205–218.

Naimie, C., 1996. Georges Bank residual circulation during weak and strong stratification periods: prognostic numerical model results. Journal of Geophysical Research 101, 6469–6486.

Naimie, C., Limeburner, R., Hannah, C., Beardsley, R., 2001. On the geographic and seasonal patterns of the near-surface circulation on Georges Bank — from real and simulated drifters. Deep-Sea Research II 48, 501–518.

Petrie, B., Dean-Moore, J., 1996. Temporal and spatial scales of temperature and salinity on the Scotian Shelf. Technical Report Canadian Technical Report of Hydrography and Ocean Sciences 177, Bedford Institute of Oceanography, Dartmouth, Nova Scotia.

Pinel-Alloul, B., Pont, D., 1991. Spatial distribution patterns in freshwater macrozooplankton: variation with scale. Canadian Journal of Zoology 69, 1557–1570.

Robinson, A., Lermusiaux, P., Sloan, N., 1998. Data assimilation. The Sea 10, 541–594.

Smith, N., 1993. Ocean modeling in a global ocean observing system. Reviews of Geophysics 31, 281–317.

Sullivan, B., Meise, C., 1996. Invertebrate predators of zooplankton on Georges Bank: 1977–1987. Deep-Sea Research II 43, 1503–1519.

U.S. GLOBEC, 1992. Northwest Atlantic implementation plan. Technical Report No. 6, U.S. GLOBEC Scientific Steering Committee Coordinating Office, Solomons, Maryland.

Wiebe, P., Beardsley, R., Mountain, D., Bucklin, A., 1996a. Global ocean ecosystem dynamics — initial program in northwest atlantic. Sea Technology 37, 67–76.

Wiebe, P., Morton, A., Bradley, A., Backus, R., Craddock, J., Arber, V., Cowles, T., Flierl, G., 1985. New developments in the MOCNESS, an apparatus for sampling zooplankton and micronekton. Marine Biology 87, 313–323.

Wiebe, P., Mountain, D., Stanton, T., Greene, C., Lough, G., Kaarvtvedt, S., Dawson, J., Copley, N., 1996b. Acoustical study of the spatial distribution of plankton on Georges Bank and the relationship between volume backscattering strength and taxonomic composition of the plankton. Deep-Sea Research II 43, 1971–2001.